Hindawi
IET Electrical Systems in Transportation
Volume 2023, Article ID 6650034, 12 pages
https://doi.org/10.1049/2023/6650034

Research Article

A Single-Stage Isolated Battery Charger Using Nonbridged Positive Cuk Converter Configuration

Tanmay Shukla,[1] **N. P. Patidar**,[1] **and Apsara Adhikari**[2]

[1]*Department of Electrical Engineering, Maulana Azad National Institute of Technology, Bhopal 462003, India*
[2]*Electrical Engineering, Kathmandu University, Dhulikhel, Nepal*

Correspondence should be addressed to Apsara Adhikari; apsara.adhikari.ku.edu@gmail.com

Received 8 June 2023; Revised 11 November 2023; Accepted 4 December 2023; Published 20 December 2023

Academic Editor: Ayman Al-Quraan

This article presents a nonbridged isolated positive Cuk (NB-IPCuk) converter-based single-stage battery charging system (SSBCS). The architecture of the suggested charger ensures the intrinsic advantage of power quality improvement in discontinuous current conduction (DCC) mode at the supply mains. The suggested NB-IPCuk converter scheme has fewer components than other bridgeless/nonbridged Cuk converter schemes. This is because the NB-IPCuk converter is a partial integration of two Cuk converters. The usage of the Cuk converter garnishes the system with input and output inductances, which lessens supply current harmonic distortion and, thus supply terminal low pass filter requirement is eradicated. The advantages of the NB-IPCuk converter are the eradication of one inductor and multiple diodes (two back-feeding diodes), which are generally used in NB converter configurations. In place of two separate inductors, the NB-IPCuk converter uses a single secondary side output inductor. The usage of BL configuration of NB-IPCuk converter eradicates the bridge rectifier (BR) stage, and thus, the BR-associated losses also got eradicated. The NB-IPCuk converter also garnishes the system with electrical isolation which adds to the safety standards of the system. DCC mode operation of the NB-IPCuk converter is used in the present work. DCC mode requires lesser sensors in comparison to continuous current conduction mode. The abovementioned benefits of the NB-IPCuk converter make the SSBCS system cheaper, compact, and more efficient. The detailed stability analysis (Bode diagram and pole-zero map) and mathematics for the NB-IPCuk converter are also included in the paper. The prototype and MATLAB/Simulink model of NB-IPCuk converter-based SSBCS system with DCC mode control has been built, and results of both prototype and MATLAB/Simulink are deployed to verify SSBCS system's performance during dynamic and steady-state conditions.

1. Introduction

Benefits like high fuel efficiency and maximum energy utilization have pushed the contemporary automotive sector toward the adoption of electric vehicles (EVs) [1]. The operation of various electrical devices linked to the grid, as well as battery performance, is significantly influenced by EV charging [2–4]. Additionally, according to the advised laws, namely the IEC 61000-3-2 standard, the battery charger's performance, i.e., sinusoidal supply current with lower distortion content in current, becomes crucial for small-scale vehicles [5]. High-quality indices, however, are hindered by the bridge rectifier's (BR) nonlinear behavior at the input of conventional battery chargers. The suggested IEC regulations are broken by the low power factor and higher harmonics content (55%–65%) in the supply current of conventional chargers. The parameters for the E-rickshaw under test and the battery rating are listed in Appendix A. In a traditional front-end power quality improvement (PQI) scheme, a converter is connected at the output terminal of the rectifier to integrate the PQI feature at the utility. The use of a second converter in a conventional battery charger, however, raises the overall component count. The efficiency and expense of the charger suffer as a result. The addition of large DC-link capacitors restricts the charger's efficiency, size, weight, and dependability in two-stage configurations for high-power applications [6]. For PQI in EV charges, a BR-fed single-stage isolated AC–DC converters are becoming more and more common [7, 8]. In the literature, various on-board battery chargers with single-phase PQI converters are documented [9]. The

on-board designs are more popular because the charger size is considerably smaller, and they offer high efficiency at high power. The interleaved PFI converter operation for high-power applications was described in the study of Musavi et al. [10]. The soft-switching techniques have become more common for greater power-operated PFI chargers [11, 12]. With the interleaved operation, the circuit inductance, electromagnetic interference (EMI) filter, and input and output ripple are all considerably reduced. Furthermore, the switch current is half that of bridged converters owing to the parallel operation of two switches. The devices' ability to dissipate heat is still limited by BR-fed charges, which puts a cap on how much they can be shrunk. Additionally, Li et al. [13] have introduced a resonant converter-based single-stage charger to capitalize on the advantages of low EMI and lower losses due to switching taken together. However, the full bridge (FB) LLC converter's operation necessitates the integration of four switches and circuitry, making the choice of converter components more demanding over a broad range of line voltage variations. In the study of Wang et al. [14], a different boost-FBLLC converter battery charger design is described. This circuit configuration has more components and is more complex. It takes a complicated control design development to create four gate drivers for devices. A number of efficient off-board-based EV charging solutions that meet the objectives of high-power density and design simplicity are described in the study of Nayak [15] and Singh et al. [16].

In EV chargers, the traditional boost rectifier is thought to be the most widely used option for integrated PQI. In unidirectional chargers, the traditional boost rectifier is thought to be the most widely used option for integrated PFC. Conventional buck [17] and boost [18] converters, on the other hand, are found to be inadequate at high power because of bad current shaping and a limited duty cycle range at varying line voltages, respectively. On the other hand, the buck-boost converter [19] has none of these drawbacks because the duty cycle can be adjusted to a broad range to account for sudden changes in mains voltage.

However, even with nonbridged (NB) technology, the buck-boost converter in the study of Siu and Ho [19] lacks separation. The aforementioned buck-boost converter's limited voltage step-down capacity and nonisolated structure make it unsuitable for single-stage charging (a subsequent isolated stage is required at the battery end). A thorough overview of the various single-phase PQI converters, including flyback, single-ended primary inductor converter (SEPIC), Cuk, and zeta converters, based on a buck-boost configuration, has been provided [20–24]. Landsman converter-based charger is presented in the study of Kushwala and Singh [25]. Due to the shortcomings of discontinuous input and output current, the single-stage isolated zeta and SEPIC converters are not appropriate for PFI at the input of battery chargers. If the input ripple is linked to the output, this requires a bulky filter, which reduces battery life. Due to the advantages of low ripples at input and output, the Cuk converter escapes any such restriction [26]. Furthermore, by using the topology in conjunction with a topology that has a continuous output current, such as a Cuk converter, the discontinuity in the output current in the SEPIC converter case can be prevented [26]. In order to enhance PQ, it seems that the two topologies combined offer the best chances. In the present work, a nonbridged isolated positive Cuk (NB-IPCuk) converter-based single-stage electrical vehicle battery charging system (SSBCS) is presented in Figure 1. The advantage of using an NB-IPCuk converter are elimination of one stage, isolated AC–DC converter, BR, one inductor, and three diodes with respect to conventional BL-Cuk converter-based charger.

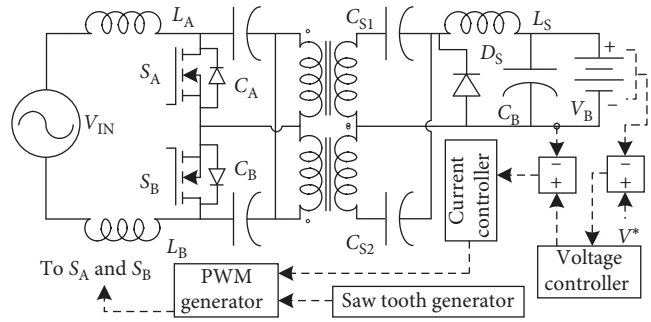

FIGURE 1: Power quality improvement NB-IPCuk converter-based SSBCS system.

Below is a list of the benefits and standout characteristics of the presented NB-IPCuk converter-based SSBCS.

(1) The main benefit of NB-IPCuk converter-based SSBCS is the elimination of the second stage, which increases the component counts of the system and makes it bulkier.

(2) NB-IPCuk converter itself presents a number of benefits over other chargers, like the eradication of an inductor and three diodes with respect to other BL-Cuk converter schemes, which reduces the cost as well as the size of the system. The NB-IPCuk converter also garnishes the single-stage system with electrical isolation.

(3) The inductor at both the terminals of the converter increases the battery current and supply current profile by eradicating the harmonics upto a significant extent, and thus, the filter need at the terminals gets extinct.

(4) PQI is achieved with a simple and noncomplex control technique. Discontinuous current conduction (DCC) mode operation of SSBCS reduces the sensor requirement, which ultimately reflects to the lower cost of the system.

(5) The presence of symmetry in operating circuits in both semicycles of input voltage lessens the analysis as well as a calculative burden to 50%, and also, to understand the working of NB-IPCuk converter, analysis of any semicycle would be sufficient due to symmetry.

2. Configuration of NB-IPCuk Converter for SSBCS

The NB-IPCuk converter is a semi-integration of two Cuk converters. The advantage of using Cuk converter is continuous input and output current, unlike SEPIC and Zeta

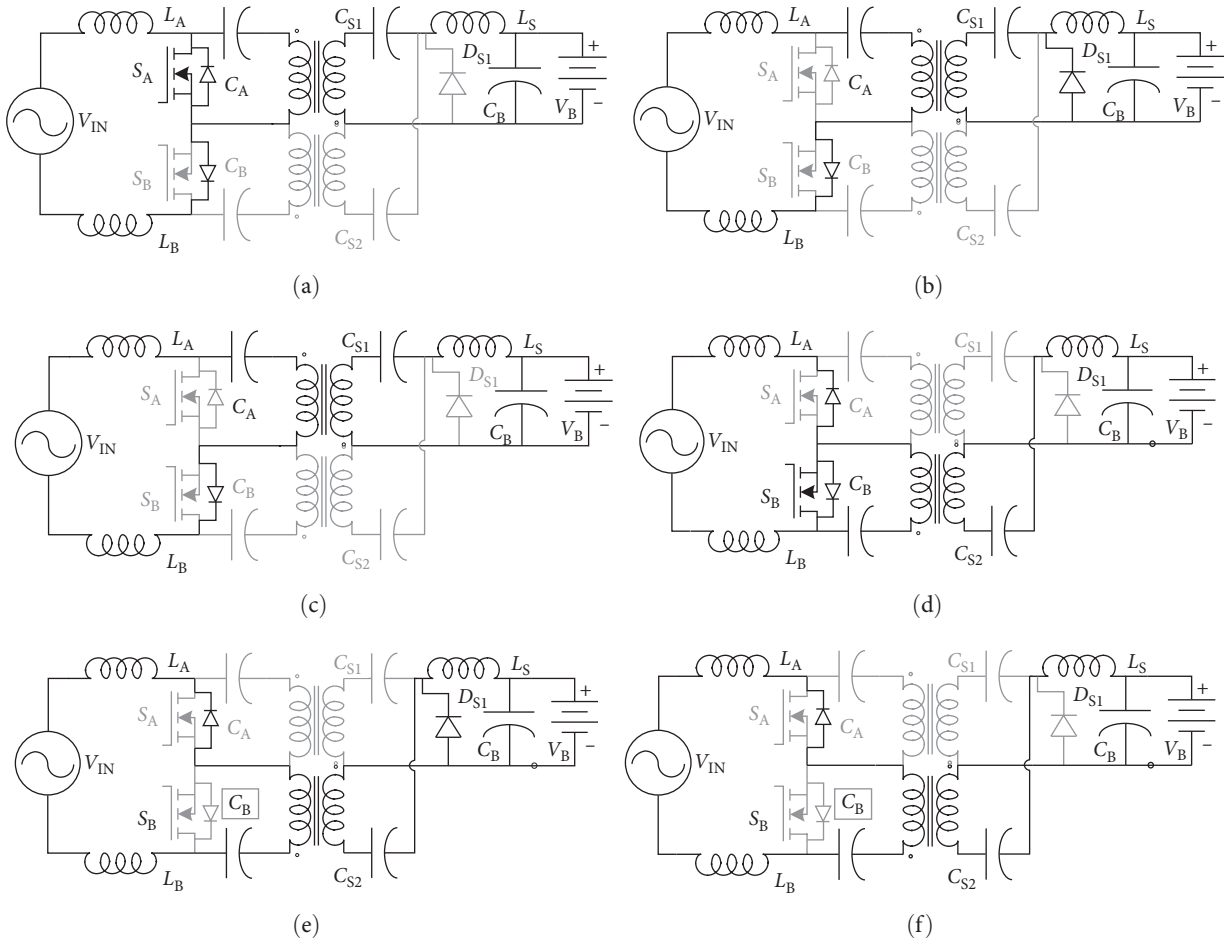

FIGURE 2: DCC mode, NB-IPCuk converter operation during (a) S_A conduction mode, (b) S_A nonconduction mode, (c) DCC operation mode (positive semicycle), (d) S_B conduction mode, (e) S_B nonconduction mode, (f) DCC-mode (negative semicycle).

converters. The Cuk converter also presents the benefit of the presence of inductance at both terminals of the converter. The inductor presence eradicates the requirement of filters at both the terminals of the converters.

2.1. NB-IPCuk Converter Operating Modes. The DCC operation mode of the NB-IPCuk converter has been elaborated in the current section. For NB-IPCuk converter DCC mode operation, a total of six scenarios exist: three occur during the input voltage's negative cycle, and the remaining three occur during its positive cycle. In this part, only positive half-cycle operation is covered due to symmetry in the NB-IPCuk converter architecture. However, Figure 2(a)–2(f) illustrates the conduction loop in each of the six potential scenarios.

The DCC mode-operated NB-IPCuk converter's six scenarios/cases are as follows:

(i) Positive semicycle of the supply voltage.
  (1) Switch S_A is on or conducting (supplied with gate pulse).
  (2) Switch S_A is off or nonconducting.
  (3) Switch S_A is off, and also diode current through diode D_A vanishes (DCC mode operation of positive cycle).

(ii) Negative half cycle of supply AC mains voltage
  (4) Switch S_B conducts.
  (5) S_B does not conduct.
  (6) S_B does not conduct, and also, inductor L_B power vanishes (DCC mode operation of negative cycle).

In this part, various operational scenarios/cases during positive semicycles are explained in order to clarify how the NB-IPCuk converter functions in DCC mode.

(1) Mode-I—For improved comprehension and clarity, Figure 2(a) shows the conduction paths during this mode. Mode-I witnessed the conduction through switch S_A. The following relation can be used to determine the input inductor current:

$$V_L = L\frac{di_L}{dt}. \tag{1}$$

Switch S_A acts as a short-circuit in this mode; the conduction loop formed in Mode-I are L_A-S_A-L_B-V_{IN}-L_A, L_A-C_A-L_{P1}-L_A, and L_{SI}-C_{S1}-D_{S1}-C_B||Load-L_{SI}.

Where L_{P1} and L_{S1} are the primary and secondary inductance of transformer positive semicycle transformer, respectively.

The maximum current through switch S_A during Mode-I is given by the equation as follows:

$$i_{SA\_Max} = \frac{V_{IN} d_\alpha T_s}{L_A + L_B} - \frac{V_{CA} d_\alpha T_s}{L_{P1}}, \quad (2)$$

where T_s and d_α are time interval and duty cycle, respectively.

(2) Mode-II—Switch S_A is turned off in this mode, and conduction paths are displayed in Figure 2(b). The diode D_{S1} conducts in Mode-II. The loops formed during this mode are V_{IN}-L_A-C_A-L_{P1}-L_B-V_{IN}, C_{S1}-L_{S1}-D_{S1}-C_{S1}, and L_S-C_B||Load-D_{S1}-L_S. Diode D_{S1} current can be found using the following:

$$i_{DS1\_max} = -\left[\frac{(V_{CS1}) d_\beta T_s}{L_{S1}} + \frac{(V_{CB}) d_\beta T_s}{L_S}\right], \quad (3)$$

where $d_y = \frac{\text{Time elapsed in Mode-II}}{T_S}$

The maximum voltage across switch S_A is given as follows:

$$V_{SA\_max} = (V_{IN} + V_{LA}) - V_{LB}. \quad (4)$$

In this operating mode, the switch S_B antiparallel diode conduction can be verified.

(3) Mode-III—The diode D_{S1} current vanishes in this mode. The current through the inductor falls to a negative value after crossing zero value and becomes equal to current through capacitor C_{S1}. The conduction paths of Mode-III are deployed in Figure 2(c). The conduction paths during DCC mode are V_{IN}-L_A-C_A-L_{P1}-L_B-V_{IN}, L_S-C_{S1}-L_{S1}-C_B||Load-L_S.

Mathematically, DCC mode may be represented as follows:

$$d_\alpha T_s + d_\beta T_s < T_s, \quad (5)$$

where $d_{ON} = d_\alpha$ and $d_{OFF} = d_\beta + d_{DCC}$

Also,

$$d_\alpha + d_\beta + d_{DCC} = 1. \quad (6)$$

Due to the symmetrical NB-IPCuk converter scheme, similar behavior can be realized for the next half cycle of the input voltage. DCC mode waveform for the positive semicycle's three operating stages of the NB-IPCuk converter is deployed in Figure 3.

2.2. SSBCS System's Differential Factors. SSBCS system's differential factors are a single-stage isolated converter-based charging scheme, PQI, rectifier elimination, component count reduction, simple control, availability of output inductances terminal inductances, elimination of filter requirements, and a simple control algorithm for DCC mode operation. A brief comparison of various BL converter-based system is tabulated in Table 1. It shows the total components count along with required switches, diodes (D), capacitors (C), inductors (L), and transformers (X).

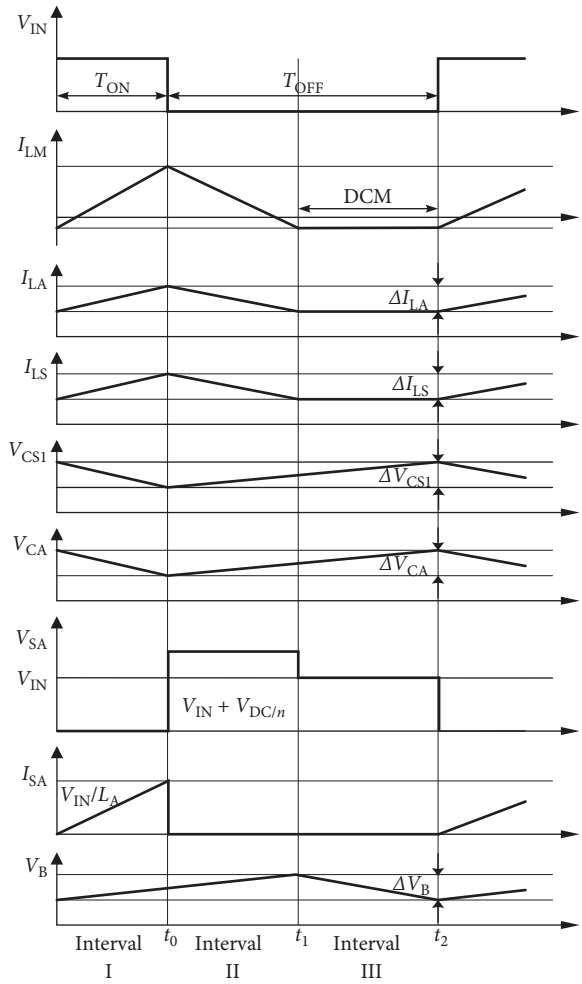

FIGURE 3: DCC mode waveform for positive semicycle's three operating stages of NB-IPCuk converter.

2.3. Components Selection and Designing for NB-IPCuk Converter. The power factor improvement NB-IPCuk converter can be operated in DCC mode only if the inductor energy completely vanishes during the T_{OFF} time of both semicycles. The SSBCS at MATLAB platform is validated in the current article using a 48 V 100 Ah lead-acid battery. The expression for the supply voltage is given as follows:

$$V_{IN} = V_M \sin(\omega_L t) = 220\sqrt{2}\sin(2\pi f_L t), \quad (7)$$

where V_m and ω_L resemble maximum supply voltage and line frequency (radian/s), respectively.

Table 1: Comparative analysis of NB-IPCuk converter with different existing BL configurations.

S. no.	Configuration	Device count					
		L	C	X	D	Switch	Total
1.	NB-Landsman [25]	4	4	1	5	2	16
2.	NB-Cuk [20]	6	6	1	5	2	20
3.	NB-SEPIC [21]	4	6	1	5	2	16
4.	NB-Luo [22]	4	4	1	5	2	16
5.	NB-Sheppard Taylor [23]	4	4	1	11	4	24
6.	NB-IPCuk converter	3	5	2	3	2	15

Now, the instantaneous value across the switch and inductor combination can be calculated as follows:

$$V_{\mathrm{IN}}(t) = |V_{\mathrm{m}}\sin(\omega_{\mathrm{L}}t)| = \left|220\sqrt{2}\sin(314t)\right|. \tag{8}$$

Transfer function (TF) of the NB-IPCuk converter can be gained by applying the voltage and second balance across the inductors. NB-IPCuk converter TF is calculated as follows:

$$\frac{V_{\mathrm{B}}}{V_{\mathrm{IN}}} = \frac{N_2}{N_1} \times \frac{d_\Psi}{1 - d_\Psi}, \tag{9}$$

where DC-link voltage is an output of the NB-IPCuk converter taken as 65 V with duty cycle d_x. The instantaneous value of $d_\psi(t)$ is dependent on voltage at DC-link and input voltage's instantaneous reading.

$$d_\Psi(t) = \frac{V_{\mathrm{CB}}}{V_{\mathrm{CB}} + V_{\mathrm{IN}}(t)} = \frac{V_{\mathrm{CB}}}{V_{\mathrm{CB}} + V_{\max}\sin(\omega_{\mathrm{L}}t)}. \tag{10}$$

Duty cycle, d_ψ can be represented as follows:

$$d_\Psi(t) = \frac{V_{\mathrm{CB}}}{V_{\mathrm{CB}} + V_{\mathrm{M}}}. \tag{11}$$

To provide a wide input variation during battery charging operation, the duty cycle range (d_ψ and d_ϕ) is calculated as 0.55 and 0.44 for minimum (170 V) and maximum (250 V) rms value of supply ac voltage, respectively.

Calculation of input terminal inductance value for DCC mode operation of NB-IPCuk converter does require switching frequency value selection, which is an important parameter in deciding the switching losses and also the rating and size of inductors. Greater switching frequencies cause greater switching losses across solid-state switches and necessitate a larger heat sink, while lower switching frequencies cause switching losses to decrease noticeably while increasing the value and size of the necessary inductor. In order to account for both factors, 20,000 Hz is chosen as the switching frequency for this work.

The value of input terminal inductance of the NB-IPCuk converter can be found using the relation as follows:

$$\begin{aligned} L_{\mathrm{A,B}} &= \frac{V_{\mathrm{IN\_min}}d_\Phi}{\varepsilon I_{\mathrm{IN}}f_{\mathrm{s}}} = \frac{V_{\mathrm{IN\_min}}^2 d_\Phi}{0.5 f_{\mathrm{s}} P_{\mathrm{Rated}}} = \frac{170^2 \times 0.55}{0.5 \times 20{,}000 \times 780} \\ &= 2 \times 10^{-3}\mathrm{H}. \end{aligned} \tag{12}$$

For continuous current conduction operation of the input inductance ($L_{\mathrm{A,B}}$) value chosen, 3,000 μH each.

The design of the NB-IPCuk converter for 780 W (P) is calculated in DCC mode by choosing the magnetizing inductance; such inductor current does not remain continuous over one cycle. The value can be estimated using the relation as follows:

$$\begin{aligned} L_{\mathrm{M1,M2}} &= \frac{V_{\mathrm{IN\_min}}d_\Phi}{2I_{\mathrm{IN}}f_s} = \frac{V_{\mathrm{IN\_min}}^2 d_\Phi}{2 f_s P_{\mathrm{Rated}}} = \frac{170^2 \times 0.55}{2 \times 20{,}000 \times 780} \\ &= 509 \times 10^{-6}\mathrm{H}. \end{aligned} \tag{13}$$

The value chosen for DCC mode operation is 85 μH.

The following expression can be used to calculate the energy storage capacitance in continuous capacitor voltage mode with allowed 15% of voltage ripple (β) at maximum input ac voltage value 250×1.414 and rated DC-link voltage as follows:

$$C_{\mathrm{A,B}} > \frac{V_{\mathrm{IN}}d_\Phi}{R_{\mathrm{L}}f_{\mathrm{s}}(1 - d_\Phi) \times \Delta V_{C_{\mathrm{A,B}}}} \times \left[\frac{N_2}{N_1}\right]^2. \tag{14}$$

The value of the capacitor for NB-IPCuk PFC converter $C_{\mathrm{A,B}}$ is taken as 0.9 μF.

The following equation can be used to calculate the value of the intermediate capacitor:

$$C_{\mathrm{S1}} > \frac{V_{\mathrm{B}}d_\Phi}{R_{\mathrm{L}}f_{\mathrm{s}}\Delta V_{\mathrm{B}}}. \tag{15}$$

The value of the capacitor chosen for the present work is 15 μF.

The value of capacitor at load terminal can be evaluated by the following formula:

$$\Delta V_{\mathrm{DC}} = \int i_{\mathrm{CDC}}(t) \times dt = -\frac{i_{\mathrm{CDC}}}{2\omega C_{\mathrm{DC}}} \times \sin(2\omega t), \tag{16}$$

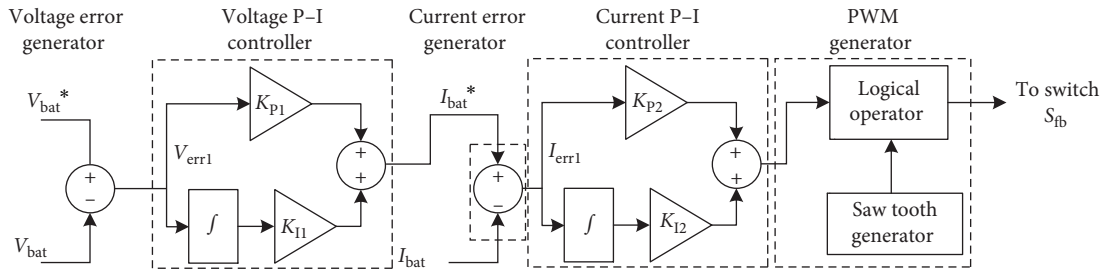

FIGURE 4: CF control loop for NB-IPCuk converter.

$$C_{DC} = \frac{i_{CDC}}{2\omega \times \Delta V_{DC}} = \frac{P}{V_{DC}} \times \frac{1}{2\omega\eta V_{DC}}, \tag{17}$$

where η equals 2%, which represents the allowed ripple in DC-link capacitor voltage. The C_{DC} value can be estimated using the following formula:

$$\begin{aligned} C_{DC} &= \frac{P}{V_{CB}} \times \frac{1}{2\omega\eta V_{CB}} \\ C_{DC} &= \frac{780}{65} \times \frac{1}{2 \times 2\pi \times 50 \times 0.02 \times 65}. \end{aligned} \tag{18}$$

The DC-link capacitor's value is set as 2.08 mF. Because the capacitor must be employed at lower switching frequencies and relatively greater current values, as well as having a higher capacitance per unit volume due to a higher capacitance value, electrolytic capacitors may be suitable for such applications.

3. Controlling of PQI NB-IPCuk Converter-Based SSBCS

The control scheme for power quality improved NB-IPCuk converter-based SSBCS is elaborated in the current section. The complete presented SSBCS scheme utilizes current follow (CF) approach.

3.1. Control Scheme for NB-IPCuk Converter. The CF control scheme is used for SSBCS. In the CF control scheme, the sensed battery voltage is compared with the reference battery voltage at the voltage error generation stage, then the generated error is processed through the voltage controller block, and its output is saturated to the rated battery current to obtain reference battery current (I_{bat}^*) during constant current charging of the battery. I_{bat}^* is again compared with the sensed battery current to generate the error. This obtained error is fed to current P–I controller to generate the duty cycle. The duty, when compared to saw tooth waves of high frequency, the gate pulse is generated. The control loop for NB-IPCuk converter-based SSBCS is shown in Figure 4.

The equation for voltage controlled loop in CI control scheme is as follows:

$$V_{err1}(n) = V_{bat}^*(n) - V_{bat}(n), \tag{19}$$

$$\begin{aligned} V_{C1}(n) = {} & V_{C1}(n-1) + K_{P1}\{V_{err1}(n) - V_{err1}(n-1)\} \\ & + K_{I1} V_{b,err1}(n), \end{aligned} \tag{20}$$

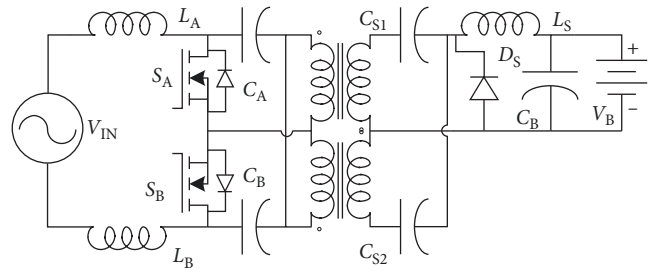

FIGURE 5: Power quality improvement NB-IPCuk converter.

where K_{P1} and K_{I1} are the voltage P–I controller's proportional and integral constants, respectively. The following is the equation for the current regulated loop:

$$I_{err1}(n) = I_{bat}^*(n) - I_{bat}(n), \tag{21}$$

$$\begin{aligned} I_{C1}(n) = {} & I_{C1}(n-1) + K_{P2}\{I_{err2}(n) - I_{err2}(n-1)\} \\ & + K_{I2} I_{b,err1}(n). \end{aligned} \tag{22}$$

The current P–I controller's proportional and integral constants are K_{P2} and K_{I2}, respectively.

4. State Space Model and Small Signal Analysis of NB-IPCuk converter

By using fundamental circuit theory laws to formulate first-order differential equations (Fo-DEs) for the conduction circuit of the NB-IPCuk converter during each conduction mode, the dynamics of the power quality improved NB-IPCuk converter can be effectively realized. These Fo-DEs are then affirmed in standard state-space form for the stability analysis of the presented NB-IPCuk converter. The standard state-space equations are as follows:

$$\left.\begin{aligned} [\dot{x}] &= [A_m][x] + [B_m][V_{IN}] \\ [y] &= [C_m][x] + [D_m][V_{IN}] \end{aligned}\right\}. \tag{23}$$

The stability analysis of positive cycle converters is only covered in this work using Bode-plot and pole–zero (P–Z) maps due to the presence of symmetry in converter configuration and a similar operation in each semi-half cycle of input voltage. Where m equals m1, m2, and m3 for the positive semi-cycle of input voltage. Figure 5 depicts the NB-IPCuk converter

undergoing a stability test used in SSBCS for improving power quality.

The matrix–vectors for the positive semicycle of the NB-IPCuk converter are as follows:

$$[A_{m1}]=\begin{bmatrix} 0 & 0 & 0 & 0 & 0 & 0 \\ 0 & 0 & 0 & \frac{-1}{L_M} & 0 & 0 \\ 0 & 0 & 0 & \frac{-1}{L_S} & \frac{-1}{L_S} & \frac{-1}{L_S} \\ \frac{1}{C_A} & 0 & \frac{1}{C_A} & 0 & 0 & 0 \\ \frac{1}{C_{S1}} & 0 & 0 & 0 & 0 & 0 \\ 0 & 0 & \frac{1}{C_A} & 0 & 0 & \frac{-1}{RC_B} \end{bmatrix},$$

$$[A_{m2}]=\begin{bmatrix} 0 & 0 & 0 & \frac{-1}{L} & \frac{-1}{L} & 0 \\ 0 & 0 & 0 & 0 & \frac{1}{L_M} & 0 \\ 0 & 0 & 0 & 0 & 0 & \frac{-1}{L_S} \\ \frac{1}{C_A} & 0 & 0 & 0 & 0 & 0 \\ \frac{1}{C_{S1}} & \frac{-1}{C_{S1}} & 0 & 0 & 0 & 0 \\ 0 & 0 & \frac{1}{C_A} & 0 & 0 & \frac{-1}{RC_B} \end{bmatrix},$$

$$[A_{m3}]=\begin{bmatrix} 0 & 0 & 0 & \left[\frac{-1}{L}+\frac{L_M}{W\times L}\right] & 0 & 0 \\ 0 & 0 & 0 & \frac{-1}{W} & 0 & 0 \\ 0 & 0 & 0 & \frac{-L_M}{WL_S} & \frac{-1}{L_S} & \frac{-1}{L_S} \\ \frac{1}{C_A} & 0 & 0 & 0 & 0 & 0 \\ 0 & 0 & \frac{1}{C_{S1}} & 0 & 0 & 0 \\ 0 & 0 & \frac{1}{C_A} & 0 & 0 & \frac{-1}{RC_B} \end{bmatrix},$$

$$[B_{m1}]=\begin{bmatrix} \frac{1}{L} & 0 & 0 & 0 & 0 & 0 \end{bmatrix}^T=[B_{m2}],$$

$$[B_{m3}]=\begin{bmatrix} \frac{1}{L}\left(1-\frac{L_M}{W}\right) & \frac{1}{W} & \frac{L_M}{WL_S} & 0 & 0 & 0 \end{bmatrix}^T,$$

$$[C_{m1}]=[C_{m2}]=[C_{m3}]=[0\ \ 0\ \ 0\ \ 0\ \ 0\ \ 1],$$

$$[D_{m1}]=[D_{m2}]=[D_{m3}]=[0], \tag{24}$$

where $L=L_1+L_2$, and $W=(LL_S+L_ML_S-L_M)$

The following relations are found after inserting the aforementioned state matrix vectors into the primary state-space equation for the positive semicycle DCC mode NB-IPCuk converter:

$$A_m=A_{m1}d_x+A_{m2}d_y+A_{m3}(1-d_x-d_y), \tag{25}$$

$$B_m=B_{m1}d_x+B_{m2}d_y+B_{m3}(1-d_x-d_y), \tag{26}$$

$$C_m=C_{m1}d_x+C_{m2}d_y+C_{m3}(1-d_x-d_y), \tag{27}$$

$$D_m=D_{m1}d_x+D_{m2}d_y+D_{m3}(1-d_x-d_y). \tag{28}$$

Now, the positive semicycle TF for the NB-IPCuk converter is expressed as follows:

$$\mathrm{TF}_{\mathrm{BL-SCC}}(+\mathrm{ve})(s)=\frac{\dot{V}_{\mathrm{DC}}(s)}{\dot{V}_{\mathrm{IN}}(s)}=\{C_m(sI-A_m)^{-1}B_m\}. \tag{29}$$

When the TF for a power quality-improved NB-IPCuk converter is calculated for DCC mode operation, it results in a TF with six poles and two zeros.

The P–Z map of TF of NB-IPCuk converter positive semicycle is deployed in Figure 6(a). The map shows six poles and only two zeros. The map also witnesses the stability of the NB-IPCuk converter by showing the positioning of all the poles either on the y-axis or on the negative second and third quadrant of coordinate axis.

For closed-loop operation, the NB-IPCuk converter is connected with P–I controller block. The TF of controller is given as follows:

$$\mathrm{TF}_C=\left[K_{\mathrm{Pr1}}+\frac{K_{\mathrm{Int1}}}{s}\right]\times\left[K_{\mathrm{Pr2}}+\frac{K_{\mathrm{Int2}}}{s}\right], \tag{30}$$

where K_{Int1} and K_{Pr1} are integral and proportional tuned parameters of the outer loop and K_{Int2} and K_{Pr2} are integral and proportional tuned parameters of the inner loop. By using the NB-IPCuk converter positive cycle TF and controller, a characteristic equation is constructed. In Figure 6(b), a Bode-plot of the entire function is presented. Large and positive values of phase margin and gain margin are found at values of 26.38° and 41.22° dB, respectively, indicates high converter (system) stability.

Similar stability can be observed for negative half-cycle converters, and because of symmetry in the BL configuration of the NB-IPCuk converter, exact findings will be obtained after using the same stability analysis method, so negative cycle converters are not explored in this study.

5. Validation and Result

The results from MATLAB/Simulink are used in this part to analyze the performance of the PQI NB-IPCuk power converter-based SSBCS under steady-state and dynamic situations.

5.1. Steady-State Performance of SSBCS. This section discusses NB-IPCuk converter-based SSBCS performance at

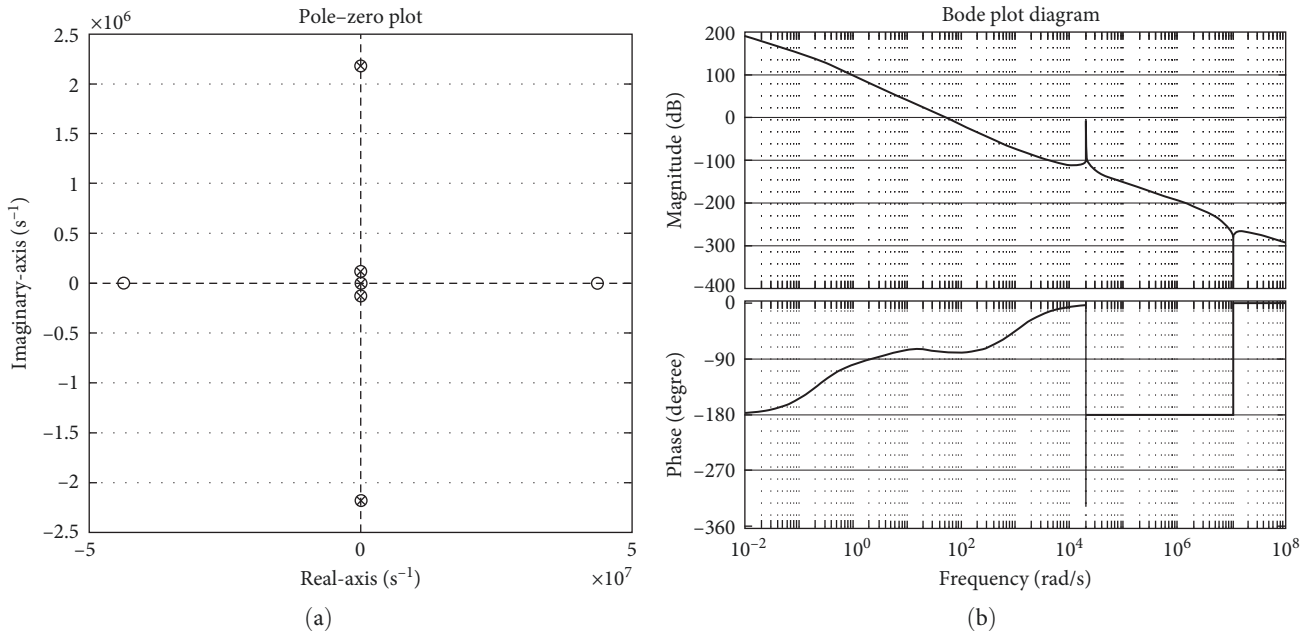

Figure 6: Positive semicycle NB-IPCuk converter analysis using (a) P–Z map and (b) Bode-plot.

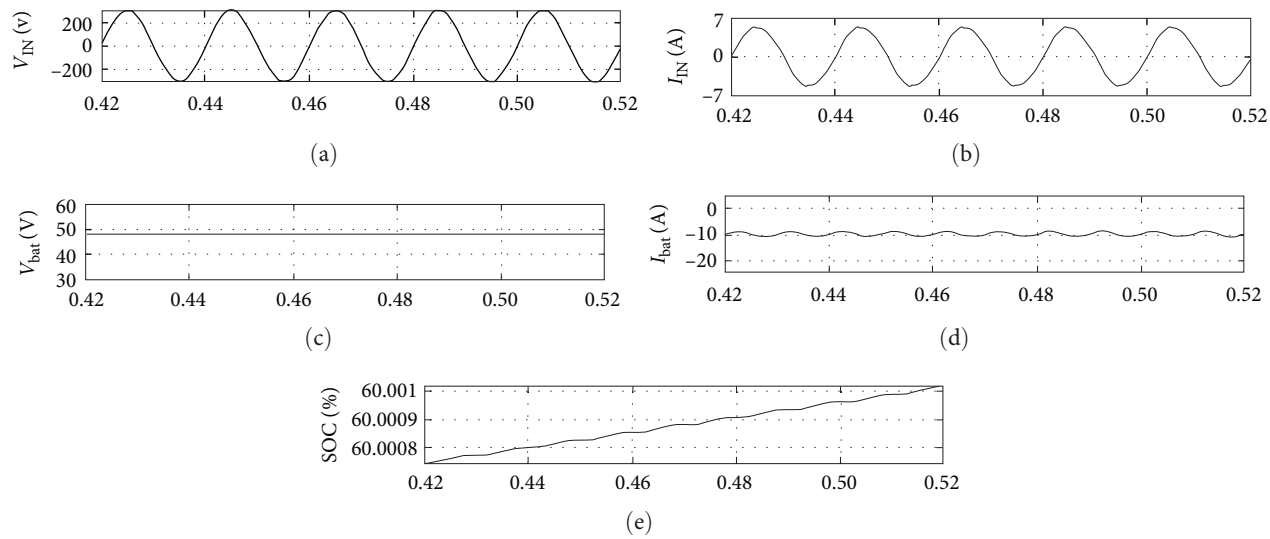

Figure 7: SSBCS performance at steady state with an input voltage of 220 V: (a) input mains voltage; (b) supply mains current; (c) V_{bat}, (d) I_{bat}, (e) SOC (%).

steady state conditions. With an input voltage of 220 V, DC-link voltage of 65 V, and battery voltage of 48 V, Figure 7(a)–7(e) represents input voltage, input current, battery voltage (V_{bat}), battery current (I_{bat}), and state of charge (SOC). The input current and input voltage clearly follow a linear relationship, as demonstrated in Figures 7(a) and 7(b). However, the battery profile can be observed in Figure 7(c)–7(e). The prototype outcome verifying the same results is deployed in Appendix B section.

5.2. PQI NB-IPCuk Converter Performance. The functionality of the NB-IPCuk converter is covered in this section. The voltage across intermediate capacitors C_A and C_B are shown in Figures 8(a) and 8(b). The maximum voltage across capacitor C_A and C_B is 714 V. The current waveforms across the inductors L_A, L_B, and L_S are depicted in Figure 8(c)–8(e), respectively. However, the switch currents are deployed in Figure 9.

5.3. PQI NB-IPCuk Converter-Based SSBCS Dynamic Performance. This section goes over the charger's dynamic performance. The effect of changing the supply voltage on the PQI NB-IPCuk converter-based charger is depicted in Figure 10. The rise in supply current is clearly noticed when the supply voltage is lowered from 220 to 162 V at instant $t = 0.34$ s and when voltage is increased back to 220 V at $t = 0.64$ s. Figure 10(c)–10(e) clearly shows despite a sudden change in supply voltage, battery charging is not significantly interrupted. The prototype outcome verifying the same results is deployed in Appendix B section.

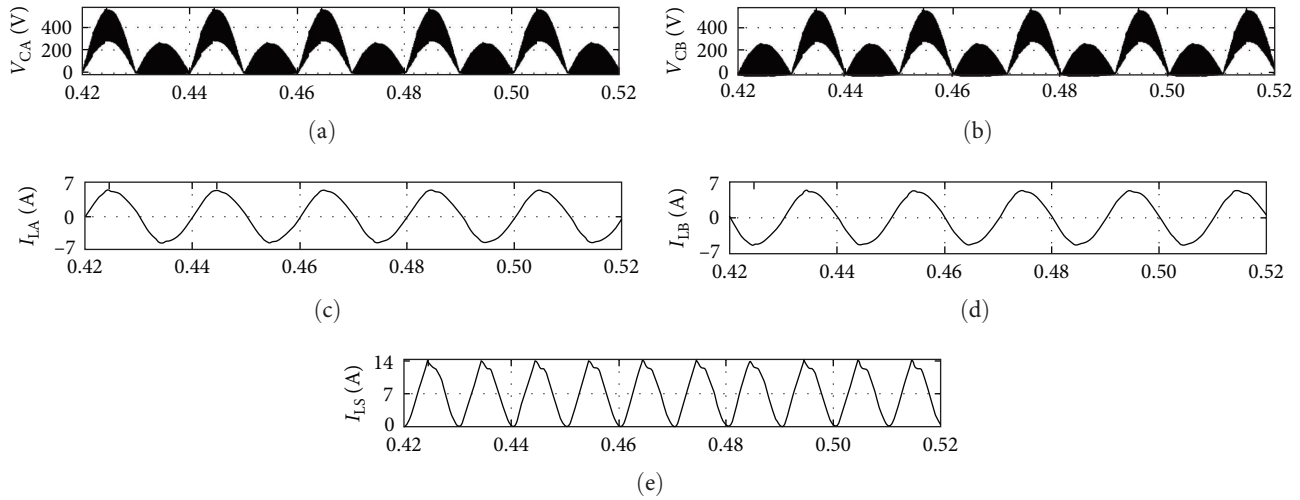

FIGURE 8: NB-IPCuk converter under steady state (a) capacitor C_A voltage, (b) Capacitor C_B voltage, (c) current through inductor L_A, (d) inductor L_B current, (e) inductor L_S current.

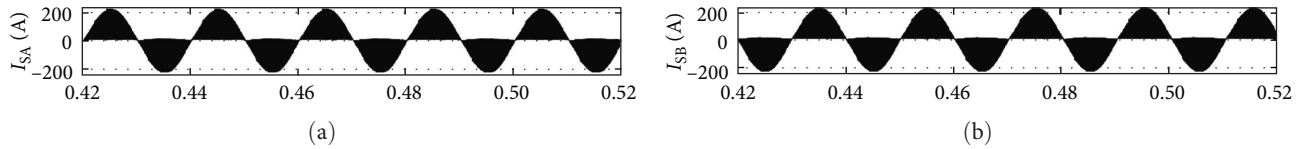

FIGURE 9: Current across NB-IPCuk converter's: (a) switch $S_{A;}$ (b) switch S_B.

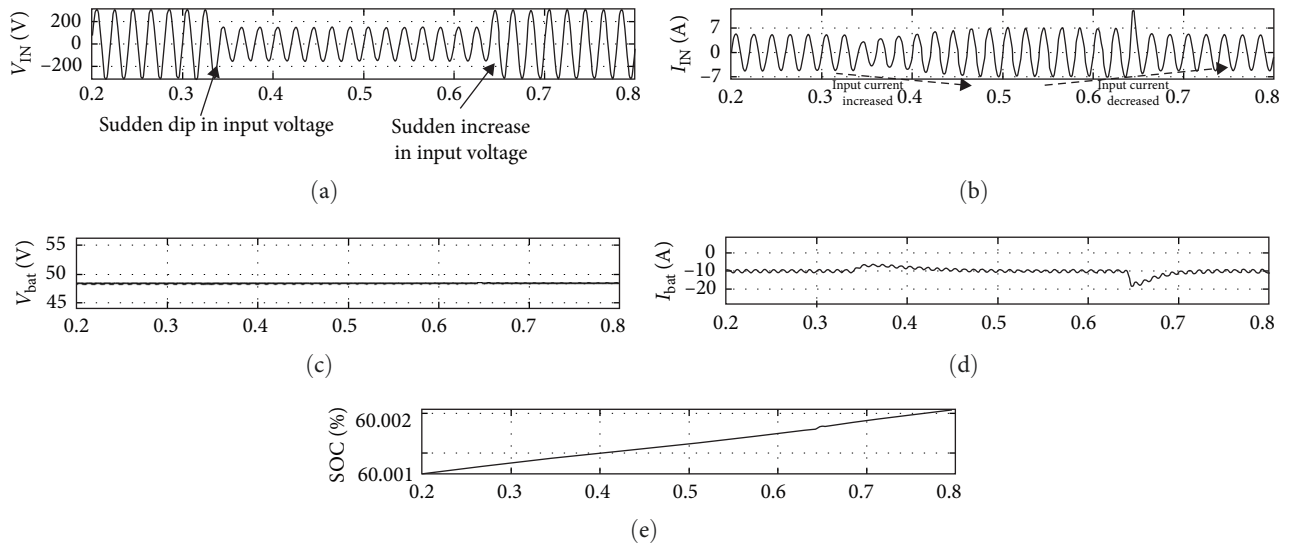

FIGURE 10: Charger dynamic performance with supply voltage step variation from 220 to 110 V at $t = 0.34$ and from 110 to 220 V at $t = 0.64$ s: (a) input voltage; (b) input current; (c) V_{bat} (battery voltage); (d) battery current (I_{bat}); (e) SOC (%).

5.4. Performance Comparison with Different Topologies. A comparison of various topologies with the presented charging system is incorporated in this section.

The topologies compared in this section are PF enhanced (PFE) Cuk with BR fed charger, PFE buck-boost with BR and filter-based charger, PFE BL-Cuk fed charger, PFE BL-buck-boost with filter-based charger, and presented isolated topology.

Figure 11 shows the efficiency variations with variations in power level for different topologies. The graphical analysis of Figure 11 certifies the lower losses in the presented topology as compared to other topologies. However, Figure 12 shows the operating power factor of different topologies at different loadings; the graphical outcomes also verify the high power factor operation of the presented charger as compared to other topologies.

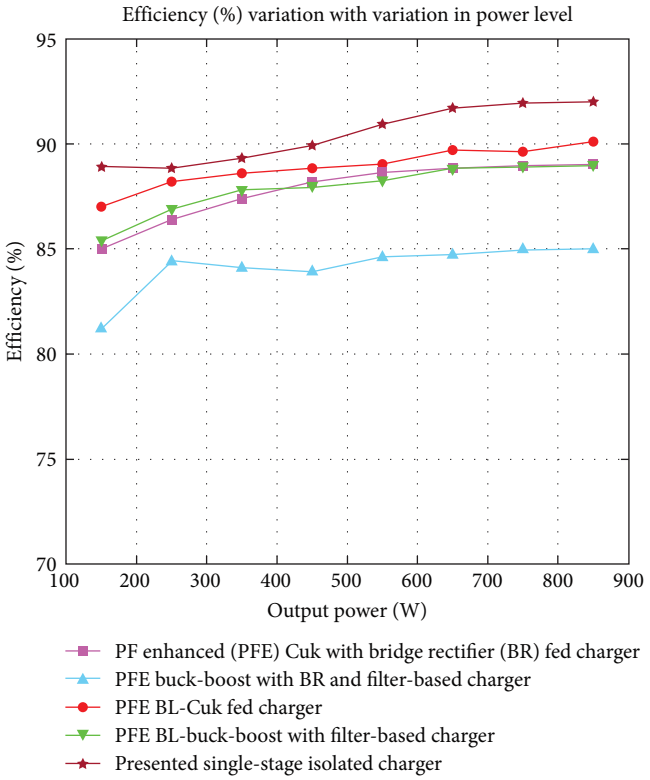

Figure 11: Efficiency curve of different topologies.

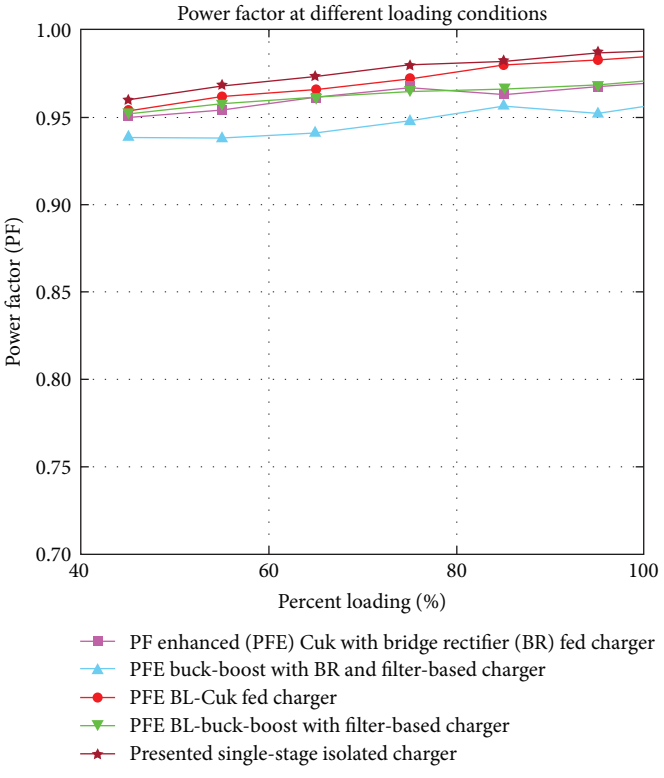

Figure 12: PF curve of different topologies at different loading conditions.

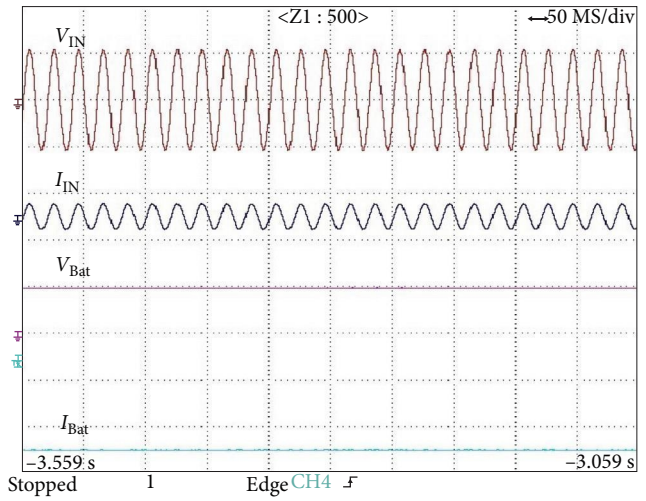

Figure 13: Steady-state prototype outcome.

6. Conclusion

This study covers the intricate mathematics and stability assessment of the NB-IPCuk converter used SSBCS. Bode diagrams and P–Z maps have been used to investigate the stability of the NB-IPCuk power factor quality improvement converter. The study has included and analyzed the simulation result from the MATLAB platform's Simulink model of SSBCS. Results from the MATLAB platform Simulink have been utilized to verify the effectiveness of a PQI NB-IPCuk converter that has better power quality, fewer components, and higher efficiency. The charger based on the NB-IPCuk converter that is being presented has a number of advantages, including size reduction and simple control. Under steady-state conditions, it is found that the input current harmonic distortion is 4.21% at 220 V RMS supply voltage. The dynamic state results appear to likewise show acceptable performance. As a consequence, the charger's overall performance has been verified using the data from the test.

Appendix

A. Parameters for the Battery and E-rickshaw under Test

Rated speed = 0–28 km/h.

Battery ratings (12 × 4 V, 100 Ah)

Charger specifications (input supply = 170–250, output current = 10–11 A, open circuit voltage = 55–58 V)

Motor specifications (48 V, 850 W BLDC motor).

B. Prototype Validation of the System

This section contains the prototype results to verify the steady state as well as the dynamic state performance of the presented SSBCS. The steady-state and the dynamic-state results of the SSBCS are shown in Figures 13 and 14, respectively. The steady-state outcomes of the SSBCS are analogous

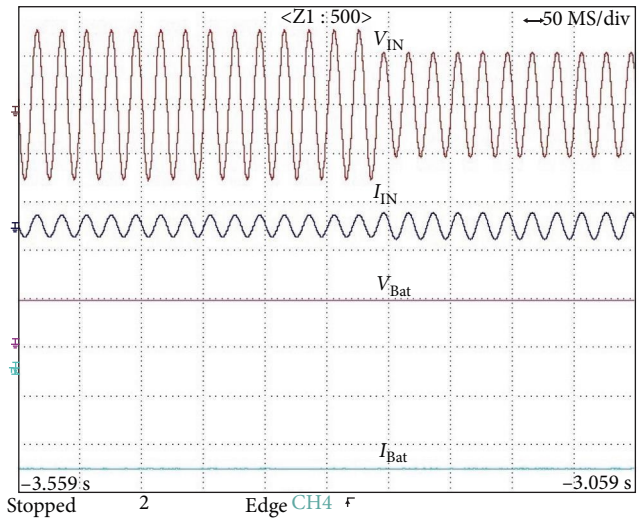

FIGURE 14: Dynamic state prototype outcome.

to the simulation model outcome in Figure 7, and the outcome of the dynamic state prototype results deployed in Figure 14 are analogous to the simulation model outcome in Figure 10.

Data Availability

Data found in the research are available in the manuscript file. The data or information used in this research are cited, and the corresponding paper details are deployed in the "Reference" section.

Conflicts of Interest

The authors declare that they have no conflicts of interest.

Authors' Contributions

Conceptualization, methodology, audit parameters, validation, investigation, and writing—original draft preparation were done by Tanmay Shukla (T.S.); formal analysis was done by T.S., N.P. Patidar (N.P.P.), and Apsara Adhikari (A.A.); resources were provided by T.S. and N.P.P.; writing—review/editing was done by T.S., A.A., and N.P.P., and supervision was done N.P.P. All authors have read and agreed to the published version of the manuscript.

References

[1] A. Emadi, M. Ehsani, and J. M. Miller, *Vehicular Electric Power Systems: Land, Sea, Air, and Space Vehicles*, Marcel Dekker, New York, NY, USA, 2003.

[2] J. Larminie and J. Lowry, *Electric Vehicle Technology Explained*, Wiley, New York, NY, USA, 2003.

[3] B. Sarlioglu, C. T. Morris, D. Han, and S. Li, "Driving toward accessibility: a review of technological improvements for electric machines, power electronics, and batteries for electric and hybrid vehicles," *IEEE Industry Applications Magazine*, vol. 23, no. 1, pp. 14–25, 2017.

[4] A. Emadi, Y. J. Lee, and K. Rajashekara, "Power electronics and motor drives in electric, hybrid electric, and plug-in hybrid electric vehicles," *IEEE Transactions on Industrial Electronics*, vol. 55, no. 6, pp. 2237–2245, 2008.

[5] International Standards IEC 61000-3-2, "Limits for harmonics current emissions (equipment current per phase)," 2000.

[6] L. Petersen and M. Andersen, "Two-stage power factor corrected power supplies: the low component-stress approach," in *APEC. Seventeenth Annual IEEE Applied Power Electronics Conference and Exposition*, vol. 2, pp. 1195–1201, IEEE, Dallas, TX, USA, 2002.

[7] J. Duarte, L. R. Lima, L. Oliveira, M. Mezaroba, L. Michels, and C. Rech, "Modeling and digital control of a single-stage step-up/down isolated PFC rectifier," *IEEE Transactions on Industrial Informatics*, vol. 9, no. 2, pp. 1017–1028, 2013.

[8] C. Li, Y. Zhang, Z. Cao, and X. Dewei, "Single-phase single-stage isolated ZCS current-fed full-bridge converter for high-power AC/DC applications," *IEEE Transactions on Power Electronics*, vol. 32, no. 9, pp. 6800–6812, 2017.

[9] F. Musavi, M. Edington, W. Eberle, and W. G. Dunford, "Evaluation and efficiency comparison of front end AC–DC plug-in hybrid charger topologies," *IEEE Transactions on Smart Grid*, vol. 3, no. 1, pp. 413–421, 2012.

[10] F. Musavi, W. Eberle, and W. G. Dunford, "A high-performance single-phase bridgeless interleaved PFC converter for plug-in hybrid electric vehicle battery chargers," *IEEE Transactions on Industry Applications*, vol. 47, no. 4, pp. 1833–1843, 2011.

[11] C. Li and D. Xu, "Family of enhanced ZCS single-stage single-phase isolated AC–DC converter for high-power high-voltage DC supply," *IEEE Transactions on Industrial Electronics*, vol. 64, no. 5, pp. 3629–3639, 2017.

[12] M. Pahlevaninezhad, P. Das, J. Drobnik, P. K. Jain, and A. Bakhshai, "A ZVS interleaved boost AC/DC converter used in plug-in electric vehicles," *IEEE Transactions on Power Electronics*, vol. 27, no. 8, pp. 3513–3529, 2012.

[13] G. Li, J. Xia, K. Wang, Y. Deng, X. He, and Y. Wang, "A single-stage interleaved resonant bridgeless boost rectifier with high-frequency isolation," *IEEE Journal of Emerging and Selected Topics in Power Electronics*, vol. 8, no. 2, pp. 1767–1781, 2020.

[14] H. Wang, S. Dusmez, and A. Khaligh, "Design and analysis of a full-bridge LLC-based PEV charger optimized for wide battery voltage range," *IEEE Transactions on Vehicular Technology*, vol. 63, no. 4, pp. 1603–1613, 2014.

[15] S. K. Nayak, "Electric vehicle charging topologies, control schemes for smart city application," in *2019 IEEE Transportation Electrification Conference (ITEC-India)*, pp. 1–6, IEEE, Bengaluru, India, 2019.

[16] A. K. Singh, A. K. Mishra, K. K. Gupta, P. Bhatnagar, and T. Kim, "An integrated converter with reduced components for electric vehicles utilizing solar and grid power sources," *IEEE Transactions on Transportation Electrification*, vol. 6, no. 2, pp. 439–452, 2020.

[17] Y. Jang and M. M. Jovanovic, "Bridgeless high-power-factor buck converter," *IEEE Transactions on Power Electronics*, vol. 26, no. 2, pp. 602–611, 2011.

[18] Y. Jang and M. M. Jovanovic, "A bridgeless PFC boost rectifier with optimized magnetic utilization," *IEEE Transactions on Power Electronics*, vol. 24, no. 1, pp. 85–93, 2009.

[19] K. K. M. Siu and C. N. M. Ho, "Manitoba rectifier—bridgeless buck-boost PFC," *IEEE Transactions on Power Electronics*, vol. 35, no. 1, pp. 403–414, 2020.

[20] R. G. A. Subramanian, K. S. Jiji, D. Chandran, and A. Abhiram, "A lead-acid battery charger using modified

bridgeless configuration of SEPIC PFC converter," in *2020 23rd International Conference on Electrical Machines and Systems (ICEMS)*, pp. 1769–1774, IEEE, Hamamatsu, Japan, 2020.

[21] R. Kushwaha and B. Singh, "A power quality improved EV charger with bridgeless Cuk converter," *IEEE Transactions on Industry Applications*, vol. 55, no. 5, pp. 5190–5203, 2019.

[22] J. Gupta and B. Singh, "Bridgeless isolated positive output Luo converter based high power factor single stage charging solution for light electric vehicles," *IEEE Transactions on Industry Applications*, vol. 58, no. 1, pp. 732–741, 2022.

[23] V. Bist and B. Singh, "A PFC based bridgeless Sheppard-Taylor converter fed brushless DC motor drive," in *2014 Innovative Applications of Computational Intelligence on Power, Energy and Controls with their impact on Humanity (CIPECH)*, pp. 262–267, IEEE, Ghaziabad, India, 2014.

[24] B. Singh, S. Singh, A. Chandra, and K. Al-Haddad, "Comprehensive study of single-phase AC–DC power factor corrected converters with high frequency isolation," *IEEE Transactions on Industrial Informatics*, vol. 7, no. 4, pp. 540–556, 2011.

[25] R. Kushwaha and B. Singh, "Power factor improvement in modified bridgeless landsman converter fed EV battery charger," *IEEE Transactions on Vehicular Technology*, vol. 68, no. 4, pp. 3325–3336, 2019.

[26] R. Kushwaha, B. Singh, and V. Khadkikar, "An isolated bridgeless Cuk–SEPIC converter-fed electric vehicle charger," *IEEE Transactions on Industry Applications*, vol. 58, no. 2, pp. 2512–2526, 2022.